Stick-Slip and Slip-Slip Operation of Piezoelectric Inertia Drives – Part II: Frequency-Limited Excitation[☆]

Matthias Hunstig*, Tobias Hemsel*, Walter Sextro*

Mechatronics and Dynamics, University of Paderborn, Pohlweg 47 - 49, 33098 Paderborn, Germany

Abstract

This contribution provides a systematic investigation and performance comparison of different modes of operation for piezoelectric inertia drives. The movement of these motors is classically assumed to consist of steps involving stiction and sliding, resulting in the term "stick-slip drives". In the first part of this contribution it has been found that using ideal driving signals, "slip-slip" operation without phases of stiction allows very high velocities, while the maximum velocity is limited principally in stick-slip operation. In this part it is shown that slip-slip operation is also suitable for use with real actuators, driven with frequency-limited versions of the ideal signals presented in part I. The motional performance of the motor as well as its wear and the required electric power are investigated for operation with different signals. It is found that for high velocity inertia motors it is recommendable to use actuators with large stroke and to drive them with a signal consisting of two harmonics at a high fundamental frequency, a result that is supported by similar setups implemented experimentally by other authors. Using Lanczos' σ factors to calculate the frequency-limited excitation signals instead of standard Fourier series additionally increases the motor performance significantly. The results help motor designers to choose the appropriate mode of operation and to optimise the motor parameters for their individual applications.

Keywords: inertia motor, stick-slip drive, mode of operation, performance indicator, velocity maximisation, actuator stroke

*Corresponding author. Telephone: +49 5251 60 1813; fax: +49 5251 60 1803; e-mail: matthias.hunstig@upb.de

Email addresses: matthias.hunstig@upb.de (Matthias Hunstig), tobias.hemsel@upb.de (Tobias Hemsel), walter.sextro@upb.de (Walter Sextro)

Accepted manuscript, submitted to Sensors and Actuators A: Physical, 13 November 2012

1. Introduction

Piezoelectric inertia motors, also known as "stick-slip drives", use the inertia of a body to drive it by means of a friction contact in small steps. The fact that these motors can also successfully operate without phases of static friction in "slip-slip" mode, demonstrated for example by motors operating in both stick-slip and slip-slip mode [1, 2, 3], has been gaining wider recognition since only a few years. Together with its first part, this contribution provides a systematic investigation of the different modes of operation of inertia motors and of the motor performance achievable in these modes.

In the first part of this contribution [4], different modes for the operation of inertia motors and the maximum motor performance achievable in these modes under ideal conditions have been investigated systematically. Prerequisites and results are briefly summarised in sections 2 and 3. In this part, frequency-limited excitation signals that are realisable with real actuators are derived from the ideal signals and the motor performance with these signals is investigated, considering the influence of actuator stroke and bandwidth.

As they are derived assuming an ideal actuator with unlimited velocity and acceleration, the performance of the motor with the ideal signals from [4] defines an upper boundary for the performance of real motors. In section 4, frequency-limited excitation signals suitable for real actuators with limited dynamics are derived from the ideal signals. In section 5, the use of inertia motors for force generation, which is not in the focus of this article, is briefly discussed. Additional to the motional performance indicators introduced in [4], section 6 defines performance indicators describing the velocity to input power ratio and the durability of the motor. The performance of motors driven with different frequency-limited signals is analysed in section 7. Section 8 investigates the influence of the actuator stroke and the actuator bandwidth on the motor performance. The conclusions presented in section 9 clearly show that this investigation of appropriate excitation signals for high velocity motors is helpful during the design of inertia motors for real applications.

2. Model

Figure 1(a) shows a schematic view of the investigated type of motor: A rigidly mounted – usually piezoelectric – actuator has a rod attached to its tip. A slider hangs below the driving rod. It is pressed against the rod by an additional contact force, usually resulting from elastic deformation or magnetic attraction.

In the first part of this contribution, a one degree of freedom model describing such a translational inertia motor, shown in figure 1(b), was introduced: A slider of mass m_s hangs below the driving rod. $x_R(t)$ and $x_S(t)$ are the displacements of rod and slider, respectively, F_c is the contact force between rod and slider. The friction force $F_f(t)$ acting between rod and slider is modelled using a Coulomb friction model with constant coefficients of static and dynamic

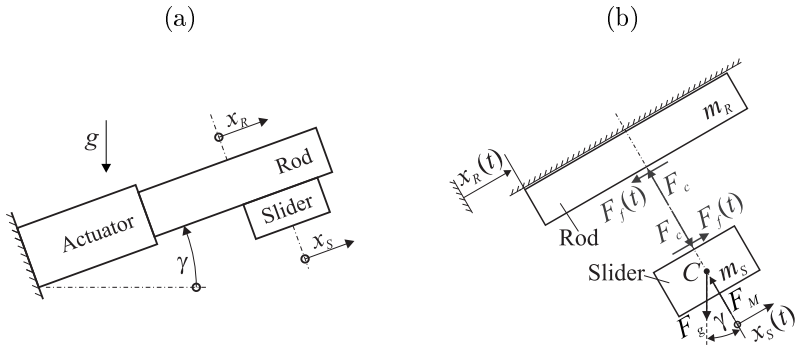

Figure 1: (a) Schematic view of a simple fixed-actuator type inertia motor and (b) rigid body model of such a motor

friction μ_0 and μ_d. The displacement of the rod is regarded as the system input, limited by the actuator stroke:

$$0 \leq x_R(t) \leq x_{R,\max} \tag{1}$$

In this model rod and slider are regarded as rigid bodies. This assumption is valid as long as the highest excitation frequency is much smaller than the first eigenfrequency of rod or slider, whichever is lower. Also, the rod is assumed to be excited purely axially and rotational effects of all forces are neglected. Only operation with slider movement in positive direction of x_S is treated in both parts of this contribution. Movement in negative direction of x_S can be treated analogously.

The investigations in both parts of this contribution are of general validity. For different diagrams and for the sample results, parameters derived from a test motor operated in the authors' lab are used. The actuator has a stroke of $x_{R,\max} = 25\,\mu\text{m}$, the slider mass is $m_S = 1.4\,\text{g}$ and the additional contact force is $F_M = 1\,\text{N}$. More details of model and motor can be found in [4].

3. Ideal excitation signals

In the first part of this contribution [4], four types of drive signals $x_R(t)$ that maximise the steady state velocity of the slider under different requirements have been described which result in different modes of operation of the motor. The differences between the four identified modes are whether the slider is accelerated by stiction or sliding friction and whether it is making discrete steps or continuously moving. The maximum velocity reachable in stick-slip operation and/or with discrete steps is limited principally, while continuous slip-slip operation allows very high velocities.

All ideal excitation signals derived in [4] contain a phase during which the driving rod is accelerated with a constant acceleration $a_R = \ddot{x}_R(t) = \kappa a_0^+$, where a_0^+ is the break-away acceleration above which the slider starts to slide.

In modes with discrete steps, this is followed by a phase with $\ddot{x}_R(t) = 0$. κ is an important parameter in the following investigations.

4. Frequency-limited excitation signals

In the first part of this contribution [4], an infinitely dynamic ideal actuator was assumed which is able to perfectly reproduce the ideal excitation signals. But real actuators show limited dynamics and let only signal components below a certain frequency pass approximately unaltered while higher frequency components are modified in both amplitude and phase. It is therefore advantageous to reduce the maximum frequency present in the voltage signal before it is fed into the actuator. This also reduces the requirements for the amplifier driving the actuator and simplifies a possible compensation of the actuator dynamics [5] because fewer frequency components have to be considered. Therefore frequency-limited signals for driving inertia motors are derived in the following, based on the ideal signals presented in the first part of this contribution.

Every periodic signal can be described as a Fourier series. Ending the Fourier series after a finite number of elements produces a frequency-limited signal which is the least-squares approximation of the original signal [6, pp. 473-474].

The classic general representation of a Fourier series of a signal with period 2π is

$$f(x) = \frac{a_0}{2} + \sum_{k=1}^{\infty} a_k \cos(kx) + b_k \sin(kx) \tag{2}$$

where the Fourier coefficients are defined as

$$a_k = \frac{1}{\pi} \int_0^{2\pi} f(x) \cos(kx)\, \mathrm{d}x, \tag{3}$$

$$b_k = \frac{1}{\pi} \int_0^{2\pi} f(x) \sin(kx)\, \mathrm{d}x. \tag{4}$$

Another form is the spectral or harmonic representation

$$f(x) = \frac{a_0}{2} + \sum_{k=1}^{\infty} d_k \sin(kx + \varphi_k) \tag{5}$$

with

$$d_k = \sqrt{a_k^2 + b_k^2}, \tag{6}$$

$$\tan \varphi_k = \frac{a_k}{b_k}. \tag{7}$$

The general form of a real displacement signal $x_R(t)$ for inertia motors with a fundamental frequency ω_0 can thus be written as a function of time t as

$$x_R(t) = \frac{a_0}{2} + \sum_{k=1}^{n} d_k \sin(k\omega_0 t + \varphi_k) \tag{8}$$

where n is the length of the Fourier series, $\boldsymbol{d} = \begin{pmatrix} d_1 & d_2 & \dots & d_n \end{pmatrix}$ is the vector of Fourier coefficients describing the amplitudes, and $\boldsymbol{\varphi} = \begin{pmatrix} \varphi_1 & \varphi_2 & \dots & \varphi_n \end{pmatrix}$ is the vector describing the phase of the individual frequency components. For velocity $\dot{x}_R(t)$ and acceleration $\ddot{x}_R(t)$ follows

$$\dot{x}_R(t) = \omega_0 \sum_{k=1}^{n} d_k k \cos(k\omega_0 t + \varphi_k), \tag{9}$$

$$\ddot{x}_R(t) = -\omega_0^2 \sum_{k=1}^{n} d_k k^2 \sin(k\omega_0 t + \varphi_k). \tag{10}$$

All ideal displacement signals derived in [4] are periodic. Their shape is similar and generally defined by

$$x_R(t) = \begin{cases} \frac{a_R}{2} t^2 & 0 \le t \le t_1 \\ 0 & t_1 < t < T \end{cases} \tag{11}$$

where the signal period is $T = 2\pi/\omega_0$, and T can equal t_1 as in the continuous modes without discrete steps. For such functions, (3) and (4) give the following formulas for the Fourier coefficients, with $k \in \mathbb{N}^+$:

$$a_0 = \frac{a_R t_1^3}{3T} \tag{12}$$

$$a_k = \frac{a_R}{2\pi} \left[\frac{T t_1}{\pi k^2} \cos\left(2\pi k \frac{t_1}{T}\right) + \left(\frac{t_1^2}{k} - \frac{T^2}{2\pi^2 k^3} \right) \sin\left(2\pi k \frac{t_1}{T}\right) \right] \tag{13}$$

$$b_k = \frac{a_R}{2\pi} \left[\frac{T t_1}{\pi k^2} \sin\left(2\pi k \frac{t_1}{T}\right) - \left(\frac{t_1^2}{k} - \frac{T^2}{2\pi^2 k^3} \right) \cos\left(2\pi k \frac{t_1}{T}\right) - \frac{T^2}{2\pi^2 k^3} \right] \tag{14}$$

Figure 2 exemplarily shows ideal signals for $x_R(t)$, $\dot{x}_R(t)$ and $\ddot{x}_R(t)$ and their approximation by Fourier series with $n = 2$ and $n = 15$. While the displacement signal is approximated well already with relatively low n, larger oscillations are present in the frequency-limited velocity and acceleration signals due to the short phases where the ideal signals are infinite.

One detail to be noted, visualised in the right half of the acceleration plots in figure 2, is that the rod acceleration $\ddot{x}_R(t)$ is almost always outside the interval $\left[a_0^-, a_0^+\right]$ of the break-away accelerations due to the oscillations present in the signal. This means that there are no phases of stiction with significant length. The only exception are signals calculated with low n for a very low a_R or for discrete modes. In these cases significant phases where stiction could take place exist, one example can be seen for $n = 2$ in figure 2(a).

Another fact to be noted is that the frequency-limited signals for $x_R(t)$ show over- and undershoots that leave the allowed range of $0 \le x_R(t) \le x_{R,\max}$, thereby violating condition (1). This effect, known as the Gibbs phenomenon [7], [8, pp. 532-534], results from the discontinuity present in the ideal signal. The maximum value of the over-/undershoot, reached for $n \to \infty$, is $0.0895 \cdot x_{R,\max}$ and independent of the signal shape during the rest of the period. On the other

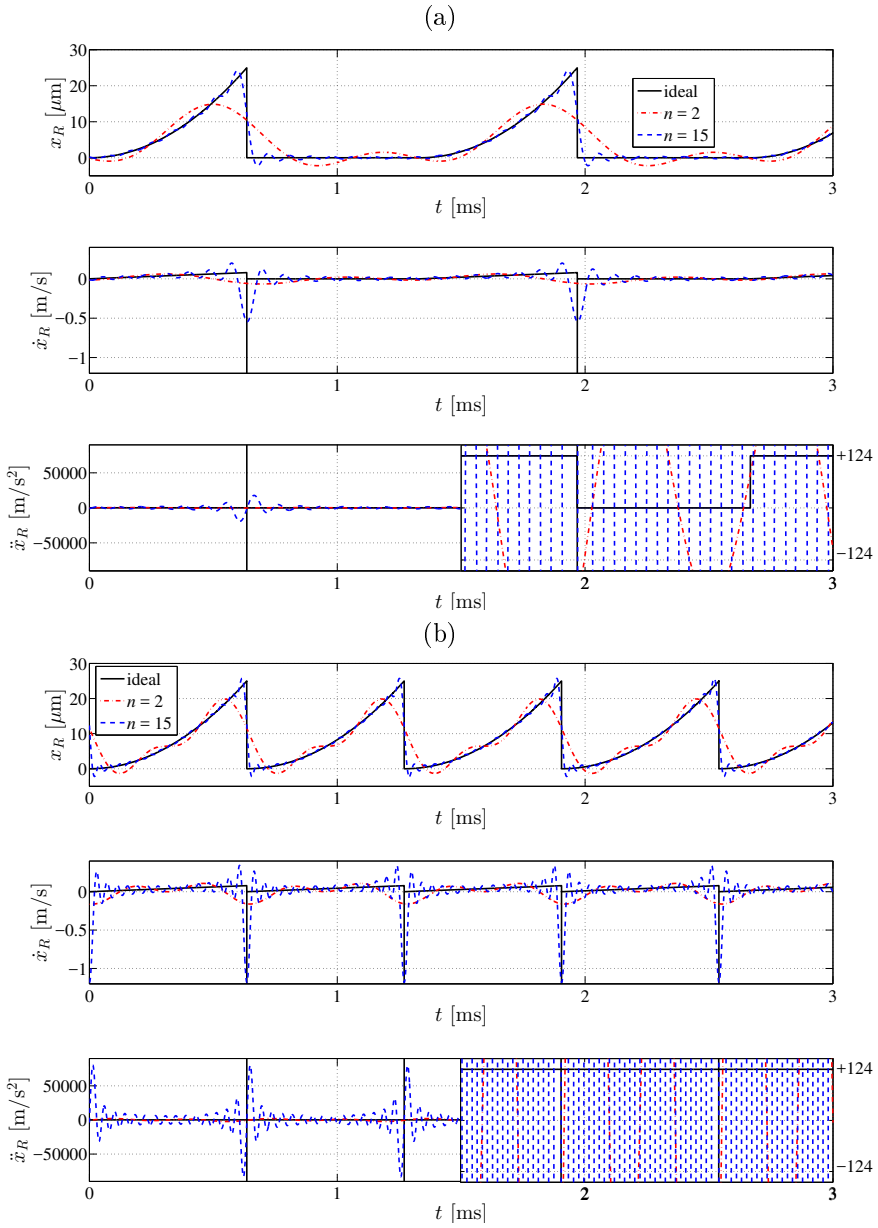

Figure 2: Ideal rod displacement, velocity and acceleration signals and their approximation with Fourier series of orders 2 and 15 for (a) discrete and (b) continuous operation (all for $\kappa = 1$). The two halves of the acceleration plots have different scales in order to visualise both the complete signals and their relation to the characteristic accelerations a_0^+ and a_0^- ($\pm 124\,\mathrm{m\,s^{-2}}$ for the example parameters).

hand, only signals with relatively high n reach values above $x_{R,\max}$, while signals with low n remain far from this maximum allowed value.

Lanczos' σ factors [8, pp. 534-538], originally developed to reduce the Gibbs phenomenon, can be used to reduce the undesired vibrations in the investigated driving signals: The Fourier coefficients are multiplied with the factors[1]

$$\sigma_k(n) = \frac{\sin\left(k\pi/(n+1)\right)}{k\pi/(n+1)} \tag{15}$$

and the modified coefficients $\sigma_k(n) \cdot d_k$ are used to calculate the frequency-limited signal. Figure 3 shows the effect of σ factors on the amplitudes of the harmonics contained in the excitation signal: With Lanczos' σ factors, the amplitudes quickly decrease to reach 0 for harmonic $n+1$ (cp. (15)), while they decrease slower and approach 0 only asymptotically without σ factors.

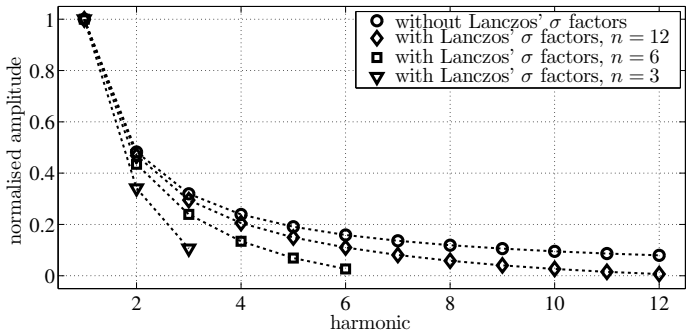

Figure 3: Normalised amplitudes d_k, respectively $\sigma_k(n) \cdot d_k$, of the harmonics contained in a signal for continuous operation as shown in figure 4 without and with Lanczos' σ factors for different n. The lines are for visual guidance only.

The σ factors have the side effect of reducing the total signal amplitude. To make maximum use of the allowed range for the actuator stroke without exceeding it, the excitation amplitude is scaled so that the real actuator stroke $\hat{x}_R = \max(x_R(t)) - \min(x_R(t))$ equals the allowed actuator stroke $x_{R,\max}$. In some of the following formulas the normalised amplitude vector $\boldsymbol{d}^* = \boldsymbol{d}/\hat{x}_R$ is used.

For all simulations described below, the excitation signal is additionally shifted so that $x_R(t)$ has a minimum of $x_R(t=0) = 0$ in order to avoid a discontinuity of $x_R(t)$ when the excitation starts from rest ($x_R(t<0) = 0$). Figure 4 shows examples of frequency-limited approximations of two ideal excitation signals with different values of n.

Figure 4 shows that the use of Lanczos' σ factors significantly reduces the undesired vibrations in the excitation signal. But even with reduced amplitude,

[1] The original definition given in [8] is $\sigma_k(n) = \sin(k\pi/n)/(k\pi/n)$, yielding $\sigma_n(n) = 0$. With this formula, the obtained signal would only contain $n-1$ harmonics. With the modified formula, it contains n harmonics as desired.

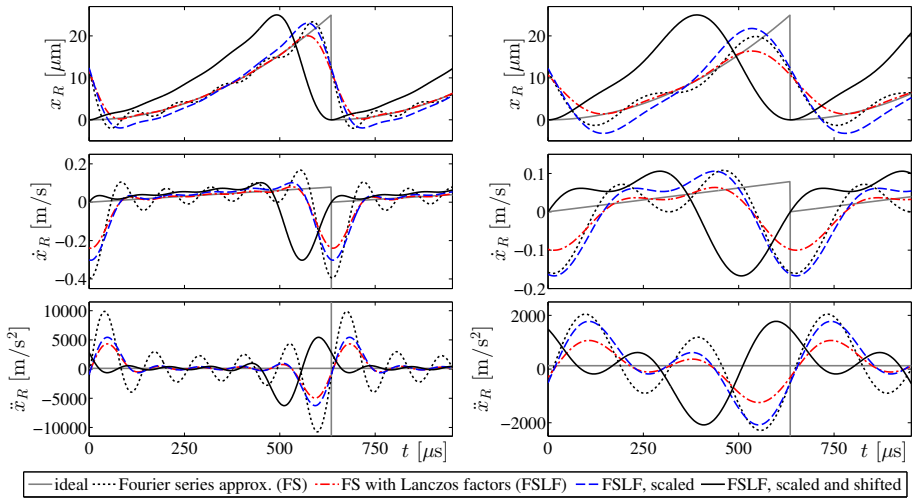

Figure 4: Rod displacement, velocity and acceleration for continuous operation ($\kappa = 1$) for $n = 2$ (left) and $n = 5$ (right)

these oscillations prevent the stick-slip motion with one phase of stiction per period found in the ideal modes of operation. The discrete stepping is the only real advantage of discrete over continuous operation, cp. [4]. The lower start-up time, which could be seen as a second advantage, directly results from the discreteness of the steps and comes at the cost of a much lower steady state velocity. The length of the phases with $x_R(t) = 0$ in the ideal discrete modes has been calculated (in [4]) to allow the slider to come to rest. With the real excitation signals, such discrete steps are hard to achieve because, due to the oscillations in the signal, the rod is never at rest, with low n not even approximately. Therefore it makes little sense to use the signals for ideal discrete operation as the basis for frequency-limited excitation signals.

This discussion shows that if stick-slip operation or discrete steps are desired, other excitation signals with much lower fundamental frequency are necessary, leading to low motor velocities. Because this contribution aims for high motor velocites, only signals derived from the ideal signals for continuous slip-slip operation are discussed in the following.

5. Force Generation with Inertia Motors

The producible force of an inertia motor can be defined and measured differently. Some authors let the slider move against some kind of spring [9, 10, 11, 12] and measure either the deformation of the spring or the spring force using a load cell connected to the other side of the spring. But it is has so far not been investigated whether the stiffness of the spring influences the result and if it makes a difference if spring and slider are rigidly connected or not, allowing collisions between the two parts. Other authors make their motor

lift weights in order to determine the producible force [13]. A third option often used for other types of piezoelectric motors [14, 15, 16] is to determine the force from the transient motor behaviour using Newton's second law. To the authors' knowledge, there has not yet been any theoretical or experimental comparison of the different methods to determine the force generated by an inertia motor.

Controlled force generation with inertia motors has only recently been investigated in more detail [9, 17, 18]. These works have shown that in the investigated motor the generated force – determined using the spring method – depends on a number of parameters such as slider mass, friction contact, preload, and excitation signal. Due to the complexity of this topic and the space a thorough investigation of force generation would require, the producible force is not investigated in this contribution and left for a future publication.

6. Performance indicators

6.1. Motional performance indicators

In the first part of this contribution [4], three indicators for the motor performance have been defined, all related to the slider movement:

- $\bar{v}_p$ is the mean slider velocity in the p-th period of the excitation signal and the steady state velocity $\bar{v}_\infty$ is defined as $\bar{v}_\infty = \lim_{p\to\infty} \bar{v}_p$.
- $T \cdot p_{0.99}$, called the start-up time, describes the time after which $\bar{v}_p \geq 0.99\,\bar{v}_\infty$.
- The smoothness indicator ς_p describes the inverse of the relative spread between minimum and maximum slider velocity in period p:

$$\varsigma_p = \frac{|\bar{v}_p|}{\max_p\left(\dot{x}_S(t)\right) - \min_p\left(\dot{x}_S(t)\right)} \tag{16}$$

  The steady state smoothness indicator is $\varsigma_\infty = \lim_{p\to\infty} \bar{\varsigma}_p$.

In a real motor, other criteria are also important, such as the power required to achieve this movement, and the lifetime of the motor. Indicators for this are derived on the following pages.

6.2. Durability indicator and friction losses

As long as they are driven within their specified operational limits, piezoelectric actuators can be designed to produce a very large number of cycles without significant degradation. [19] Thus the mechanical components are an important factor determining the lifetime of piezoelectric inertia motors. One major cause of degradation is wear in the friction contact.

According to Rabinowicz [20, p. 132-133], adhesive wear is the most common and least preventable form of wear especially in metallic contacts. For given material and surface conditions, the volume worn away by adhesive wear is approximately proportional to the load and to the distance slid [20, p. 156].

The material volume V_p worn away in the inertia motor in period p can thus be calculated as

$$V_p = w \int_{(p-1)\cdot T}^{p\cdot T} F_c \left| \dot{x}_R(t) - \dot{x}_S(t) \right| \mathrm{d}\, t \tag{17}$$

where w is a factor determined by the materials in contact and the surface conditions.

A suitable indicator for the durability of a motor is the positioning distance achieved per unit of worn volume. This value is multiplied by w to obtain the indicator δ_p for the durability of a motor which is independent of material and surface conditions:

$$\delta_p = \frac{\bar{x}_p}{V_p} w = \frac{\bar{v}_p T}{V_p} w. \tag{18}$$

The energy dissipated in the friction contact in a period p is described by

$$W_{f,p} = \int_{(p-1)\cdot T}^{p\cdot T} F_c \mu_d \left| \dot{x}_R(t) - \dot{x}_S(t) \right| \mathrm{d}\, t. \tag{19}$$

Equations (17) and (19) show that $W_{f,p}/\mu_d = V_p/w$, which means that in any given setup with fixed μ_d and w, $W_{f,p} \propto V_p$ and thus the velocity to friction power ratio $\bar{v}_p/(W_{f,p}/T)$ is directly proportional to the durability indicator δ_p. This is the case for the setups investigated in this contribution. Thus only the steady state durability indicator δ_∞ is investigated in the following.

6.3. Velocity to input power ratio

6.3.1. Assumptions

The electric power required to drive a piezoelectric actuator is highly dependent on the driving frequency. High amplitudes can be achieved with relatively low input power in resonant operation. This effect can also be used in inertia motors by combining multiple resonant modes, as shown for example by Bansevicius and Blechertas [21], Koc [22], Nishimura et al. [3], Morita et al. [23]. Determining the input power of such an inertia motor requires detailed knowledge of the specific electromechanical system and thus cannot be done generally.

In the following it is assumed that the highest frequency $f_{\max} = n/T$ contained in the excitation signal is below or around the first resonance frequency of the system, so that all frequency components of the excitation signal can be regarded as uninfluenced by higher resonances. This is the case in many inertia motors found in literature. This assumption does not mean that the response $x_R(t)/u(t)$, with the applied voltage $u(t)$, is the same for all frequency components. Indeed, the responses can be very different especially around resonance. In many cases the required electrical driving signal can be calculated relatively easily from the desired displacement signal, using either the inverted transfer function of the piezoelectric actuator or its measured frequency response, as demonstrated in [5].

As a second assumption, the friction force is regarded negligibly small compared to the inertial force $m_R \ddot{x}_R(t)$ of the driving rod for the dominant part of

the period. This assumption is valid in most inertia motors. For example, in the case shown in figure 2(b), the inertial force in the example motor, driven at a fundamental frequency of 1574 Hz with $n = 2$, reaches a maximum of 5.94 N, while the maximum possible friction force is $\mu_0 F_c = 0.19\,\mathrm{N}$.

These two assumptions allow a general closed solution for the input power of a piezoelectric inertia motor.

6.3.2. Input Power

As the piezoelectric actuator and the driving rod are rigidly connected, the movement of the actuator equals the movement of the driving rod. Up to slightly above its first resonance frequency, a piezoelectric transducer can be described with sufficient accuracy by a single degree of freedom model. Based on the notation used by Richter et al. [24, p. 111] and neglecting the usually very small electric losses inside the piezoelectric actuator, the model is described by

$$m\ddot{x}_R(t) + d\dot{x}_R(t) + cx_R(t) = F(t) + \alpha u(t) \tag{20}$$

$$q(t) - \alpha x_R(t) = Cu(t) \tag{21}$$

where m, d, c are equivalent mass, damping, and stiffness of the transducer, α is the transfer factor between electrical and mechanical domain, and C is the capacitance of the transducer. $F(t)$ is the force acting on the transducer, $q(t)$ is the charge on the tranducer and $u(t)$ is the voltage.

The transfer functions for such a system can be written in complex notation as

$$\begin{pmatrix} \hat{\underline{i}} \\ \hat{\underline{v}} \end{pmatrix} = \begin{pmatrix} \underline{y}_{11} & \underline{y}_{12} \\ \underline{y}_{21} & \underline{y}_{22} \end{pmatrix} \cdot \begin{pmatrix} \hat{\underline{u}} \\ \hat{\underline{F}} \end{pmatrix} \tag{22}$$

where $\underline{y}_{11}$ to $\underline{y}_{22}$ are different short-circuit admittances and $i(t) = \dot{q}(t) = \Re\left(\hat{\underline{i}}\exp(j\omega t)\right)$, $\dot{x}_R(t) = \Re\left(\hat{\underline{v}}\exp(j\omega t)\right)$, $u(t) = \Re\left(\hat{\underline{u}}\exp(j\omega t)\right)$, $F(t) = \Re\left(\hat{\underline{F}}\exp(j\omega t)\right)$.

For the investigated inertia motor (cp. fig 1(b)), $F(t) = -F_f(t) - m_R\ddot{x}_R(t)$. Assuming that $F_f(t)$ is negligibly small (cp. section 6.3.1) compared to the inertial force $m_R\ddot{x}_R(t)$, $F(t) = -m_R\ddot{x}_R(t)$. With this purely inertial force $F(t)$, (20) can also be written as

$$M\ddot{x}_R(t) + d\dot{x}_R(t) + cx_R(t) = \alpha u(t), \tag{23}$$

with $M = m + m_R$ and $F(t) = 0$. With $\hat{\underline{F}} = 0$, (22) becomes

$$\begin{pmatrix} \hat{\underline{i}} \\ \hat{\underline{v}} \end{pmatrix} = \begin{pmatrix} \underline{y}_{11} \\ \underline{y}_{21} \end{pmatrix} \cdot \hat{\underline{u}} \tag{24}$$

which allows to determine voltage and current required to achieve a desired velocity:

$$\hat{\underline{u}} = \frac{1}{\underline{y}_{21}}\hat{\underline{v}} \tag{25}$$

$$\hat{\underline{i}} = \frac{\underline{y}_{11}}{\underline{y}_{21}}\hat{\underline{v}} \tag{26}$$

The amplitudes of the two admittances are:

$$\left|\underline{y}_{11}\right| = \frac{\sqrt{\left(d\alpha^2\right)^2 + \left(-\left(\omega M - \frac{c}{\omega}\right)\alpha^2 + Cd^2\omega + C\left(\omega M - \frac{c}{\omega}\right)^2\omega\right)^2}}{d^2 + \left(\omega M - \frac{c}{\omega}\right)^2} \tag{27}$$

$$\left|\underline{y}_{21}\right| = \frac{\alpha}{\sqrt{d^2 + \left(\omega M - \frac{c}{\omega}\right)^2}} \tag{28}$$

So the amplitudes of voltage and current can be determined as:

$$\hat{u} = |\underline{\hat{u}}| = \left|\frac{1}{\underline{y}_{21}}\right| \hat{v} = \hat{v}\frac{\sqrt{d^2 + (\omega M - \frac{c}{\omega})^2}}{\alpha} \tag{29}$$

$$\begin{aligned}\hat{i} = \left|\underline{\hat{i}}\right| &= \left|\frac{\underline{y}_{11}}{\underline{y}_{21}}\right| \hat{v} \\ &= \frac{\sqrt{\alpha^4 - 2C\left(\omega M - \frac{c}{\omega}\right)\alpha^2\omega + C^2\left(d^2 + \left(\omega M - \frac{c}{\omega}\right)^2\right)\omega^2}}{\alpha}\hat{v}\end{aligned} \tag{30}$$

The above formulas are for monofrequent operation. In the Fourier series describing the excitation signal, the velocity amplitude for each harmonic is described by $\hat{v}_k = k\omega_0 d_k$. The amplitudes of voltage and current for each harmonic follow from (29) and (30) as

$$\hat{u}_k = \frac{\omega_0 d_k k}{\alpha}\sqrt{A_k}, \tag{31}$$

$$\hat{i}_k = \frac{\omega_0 d_k k}{\alpha}\sqrt{\alpha^4 + 2C\alpha^2\left(c - Mk^2\omega_0^2\right) + C^2k^2\omega_0^2 A_k}, \tag{32}$$

with $A_k = d^2 + \left(k\omega_0 M - c/\left(k\omega_0\right)\right)^2$ introduced for brevity. From these expressions the effective (RMS) values U and I of the total voltage and current are determined by [25, p. 14]:

$$U = \sqrt{\frac{1}{2}\sum_{k=1}^{n}\hat{u}_k^2} \tag{33}$$

$$I = \sqrt{\frac{1}{2}\sum_{k=1}^{n}\hat{i}_k^2} \tag{34}$$

The amplitude S of the complex power is

$$S = UI. \tag{35}$$

Inserting the Fourier series terms for voltage and current into (35) with (31)

and (32) leads to

$$\begin{aligned} S &= \frac{1}{2}\sqrt{\sum_{k=1}^{n}\hat{u}_k^2}\cdot\sqrt{\sum_{k=1}^{n}\hat{i}_k^2} \\ &= \frac{\omega_0^2 x_{R,\max}}{2\alpha^2}\cdot\sqrt{\sum_{k=1}^{n}\left(d_k^* k\right)^2 A_k} \\ &\quad\cdot\sqrt{\sum_{k=1}^{n}\left(d_k^* k\right)^2\left(\alpha^4+2C\alpha^2\left(c-Mk^2\omega_0^2\right)+C^2k^2\omega_0^2A_k\right)}. \end{aligned} \tag{36}$$

This term shows that the required electric power is proportional to $x_{R,\max}$ if the other actuator parameters are uninfluenced by this value. The exact dependence on ω_0 depends on the actuator parameters.

6.3.3. Velocity to input power ratio

The efficiency, defined as (mechanical) output power devided by (electric) input power, is often used to compare electric drives. But for drives mainly used for positioning it is of little use. For example, an inertia motor positioning a (freely movable) load horizontally never has a measurable useful output power: It exerts no force and the load has the same potential energy before and after positioning.

As the main target of this contribution is to enable faster inertia motors, a different indicator suitable especially for positioning applications is defined to indicate how well a motor uses its input power for generating fast movements: The velocity to input power ratio $\zeta_\infty = \bar{v}_\infty/S$, relating steady state velocity to electrical input power.

7. Performance with frequency-limited excitation signals

The results presented in the following subsection have been calculated using a numerical motor simulation. The frequent switching between stiction and sliding friction and the frequent changes of the sign of the friction force make the simulation with standard variable step algorithms very slow and can lead to numerical instabilities. In order to speed up the calculation and receive reliable results, a fixed step algorithm with 5000 time steps per period of the highest harmonic in the excitation signal was used. Evaluation of the simulation results shows that there are no significant phases of sliding friction without Lanczos' σ factors. With σ factors, the time of stiction is larger than 0.1% of the simulated time in 6 of the simulated 25 cases, the largest value reached is 3.1%. The motor thus operates almost completely using sliding friction.

For calculating the velocity to input power ratio, parameters identified for the single degree of freedom model of the piezoelectric actuator driving the above-mentioned test motor were used. Table 1 contains these parameters.

Parameter	Symbol	Value
equivalent mass (actuator + driving rod)	M	$3.2\,\mathrm{g}$
equivalent damping	d	$9.50\,\mathrm{N\,s\,m^{-1}}$
equivalent stiffness	c	$24.6\,\mathrm{N\,\mu m^{-1}}$
transfer factor	α	$1.985\,\mathrm{N\,V^{-1}}$
capacitance	C	$800\,\mathrm{nF}$

Table 1: Parameters of the single degree of freedom actuator model describing the piezoelectric actuator in the test motor, including the driving rod, used for the sample calculations in this contribution

The frequency of the highest harmonic present in the excitation signals is $f_{\max} = nf_0$, where $f_0 = 1/T$ is the fundamental frequency of the driving signal. For the continuous mode signals this becomes

$$f_{\max} = n\sqrt{\frac{a_R}{2x_{R,\max}}} = \sqrt{\kappa}n\sqrt{\frac{a_0^+}{2x_{R,\max}}}, \tag{37}$$

cp. [4]. This formula shows that while increasing n and κ increases the steady state velocity, it also increases the frequencies present in the signal. Real actuators cannot work at arbitrary frequencies but have a maximum frequency up to which they can be practically operated, so n and κ cannot be increased arbitrarily in reality. Therefore signals with equal maximum frequency $f_{\max}$ are compared in the following. For a given $f_{\max}$, choosing a higher n means to have a signal with more harmonics, but a lower fundamental frequency, as shown in figure 5.

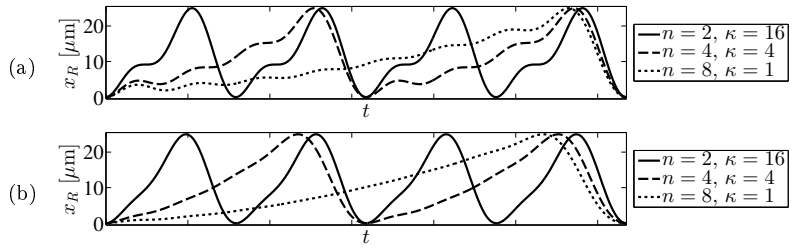

Figure 5: Different displacement signals $x_R(t)$ with equal maximum frequency $f_{\max}$, without (a) and with (b) Lanczos' σ factors.

Figures 6 and 7 show steady-state velocity $\bar{v}_\infty$, start-up time $T \cdot p_{0.99}$, smoothness ς_∞, durability indicator δ_∞, and the velocity to input power ratio ζ_∞, respectively, reached with equal $f_{\max}$ for different combinations of n and κ with and without the use of Lanczos' σ factors.

Higher maximum frequencies lead to higher steady state velocities $\bar{v}_\infty$. For any given maximum frequency the highest steady state velocity is reached with $n = 2$. Using σ factors significantly increases the steady state velocities, by between 55% and 130% in the shown cases. The maximum steady state velocity

in ideal stick-slip operation was found to be $0.06\,\mathrm{m\,s^{-1}}$ for the investigated motor [4]. In slip-slip operation using frequency-limited signals, this velocity is clearly exceeded: With σ factors and $n = 2$ it is reached already for $\sqrt{\kappa} \geq 1.5$ and for $\sqrt{\kappa} = 6$ a velocity of $0.297\,\mathrm{m\,s^{-1}}$ is reached, i. e. 495% of the maximum steady state velocity in ideal stick-slip operation.

The start-up time $T \cdot p_{0.99}$ is generally larger for larger maximum frequencies. Without σ factors, the relationship between n and $T \cdot p_{0.99}$ is steady: For any given maximum frequency, increasing n decreases the start-up time. With σ factors, the general tendency is the same, but the relationship is not steady. For example, the start-up time for $n = 3$ is shorter than for $n = 2$ or 4 in all investigated cases. Generally, the start-up time with an odd number of harmonics is shorter than with the neighbouring even numbers of harmonics. For all maximum frequencies, the minimum start-up time is reached with $\kappa = 1$.

The smoothness of the slider motion ς_∞ is generally larger for larger maximum frequencies. For any given maximum frequency, increasing n decreases the smoothness. The use of σ factors increases the smoothness for $n = 2$, has little influence at $n = 3$ and reduces the smoothness at $n \geq 4$.

Without σ factors, there is only a very small influence of the maximum frequency $f_{\max}$ on the durability indicator δ_∞. For any $f_{\max}$, it is lowest for $n = 2$, then rises with rising n. With high $f_{\max}$, it reaches a maximum above which it begins to very slowly decrease with rising n. With σ factors, the durability indicator on average is about twice as high as without σ factors and more strongly influenced by $f_{\max}$. It is generally higher for lower $f_{\max}$ and for any $f_{\max}$ it is highest for $\kappa = 1$. If durability is very important in a motor application, it can be increased by about 30% by using high values of n. But this also brings disadvantages regarding the motional performance and the effect is far smaller than what can possibly be achieved using suitable frictional materials and surfaces. Before changing the driving signal, these should therefore be the first measures to increase the lifetime of an inertia motor.

The velocity to input power ratio ζ_∞ is found to be generally higher for higher $f_{\max}$. Without σ factors, it steadily falls for rising n for high $f_{\max}$. For lower $f_{\max}$, it has a maximum at $n = 3$. Using σ factors significantly increases the velocity to input power ratio by up to 124%. With σ factors, it is higher for higher $f_{\max}$ and maximal for $n = 2$ for any $f_{\max}$.

8. Influence of actuator stroke and bandwidth

In [4] the same influence of the actuator stroke on the step size and the steady state velocity was found for all investigated ideal modes of operation (where $x_{R,\max} = \hat{x}_R$):

$$\bar{x}_\infty \propto \hat{x}_R \tag{38}$$

$$\bar{v}_\infty \propto \sqrt{\hat{x}_R} \tag{39}$$

These proportionalities are not only valid for the specific ideal and frequency-limited excitation signals derived in the previous chapters, but for any periodic

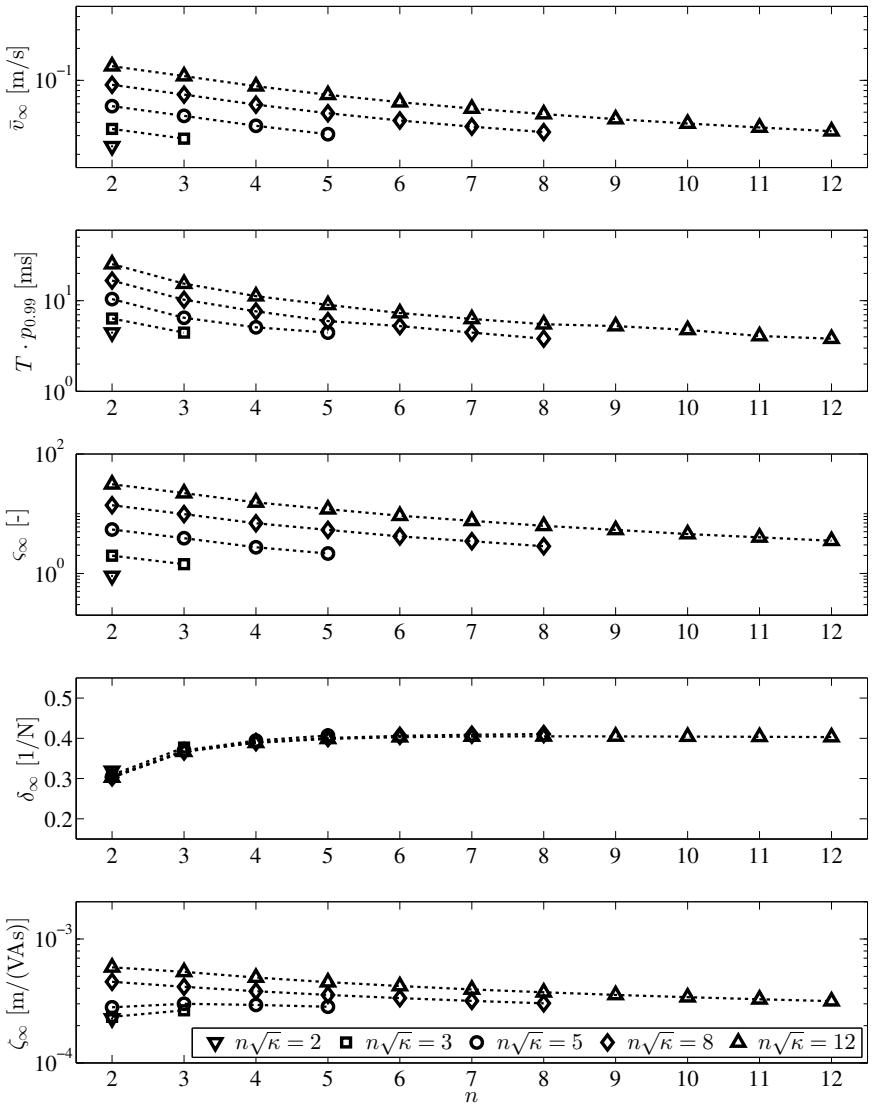

Figure 6: Steady state velocity $\bar{v}_\infty$, start-up time $T \cdot p_{0.99}$, smoothness ς_∞, velocity to input power ratio ζ_∞, and durability indicator δ_∞ for different maximum frequencies $f_{\max} \propto n\sqrt{\kappa}$, **without** Lanczos' σ factors. Results for other values of $n\sqrt{\kappa}$ are not shown, but fit the shown results without exception. The lines are for visual guidance only as $n \in \mathbb{N}^+$.

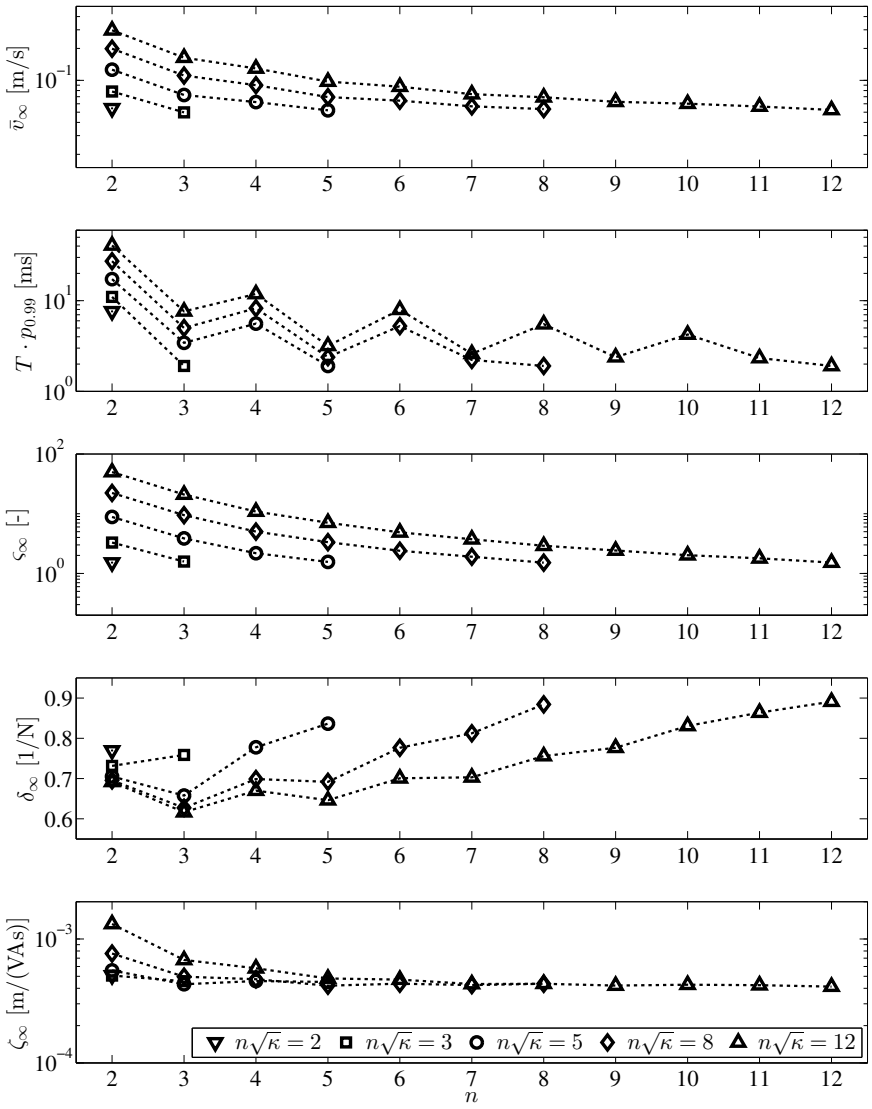

Figure 7: Steady state velocity $\bar{v}_\infty$, start-up time $T \cdot p_{0.99}$, smoothness ς_∞, velocity to input power ratio ζ_∞, and durability indicator δ_∞ for different maximum frequencies $f_{\max} \propto n\sqrt{\kappa}$, **with** Lanczos' σ factors. Results for other values of $n\sqrt{\kappa}$ are not shown, but fit the shown results without exception. The lines are for visual guidance only as $n \in \mathbb{N}^+$.

excitation signal, if the signal form, determined by the normalised amplitude vector $\boldsymbol{d}/\hat{x}_R$ and the phase vector $\boldsymbol{\varphi}$, is kept constant and the period T of the excitation signal is adjusted following the proportionality found for the ideal signals in [4]:

$$T \propto \sqrt{\hat{x}_R} \tag{40}$$

This statement is proven with the help of an example: Figure 8 shows typical velocity signals for rod and slider in steady state, excited with a frequency-limited signal ($n = 2$), over one period T. With constant $\boldsymbol{d}/\hat{x}_R$ follows for the amplitude of the rod velocity $\hat{v}_R$ from (9) and (40):

$$\hat{v}_R \propto \omega_0 \hat{x}_R = \frac{2\pi}{T}\hat{x}_R \propto \sqrt{\hat{x}_R} \tag{41}$$

Thus a change of $\hat{x}_R$ changes $\dot{x}_R(t)$ in figure 8 equally on the time and velocity axes. This means that the acceleration of the rod is unchanged. Thus the course of $\dot{x}_S(t)$, determined by the "slopes" a_d^+ and a_d^-, does not change qualitatively. Even if there are phases of stiction, the courses of the velocities of rod and slider are qualitatively unchanged by a change of $\hat{x}_R$: Because the course of the acceleration over the normalised time t/T remains the same, the break-away acceleration a_0 is reached at the same normalised times. The steady state slider velocity is thus qualitatively uninfluenced by a change of $\hat{x}_R$.

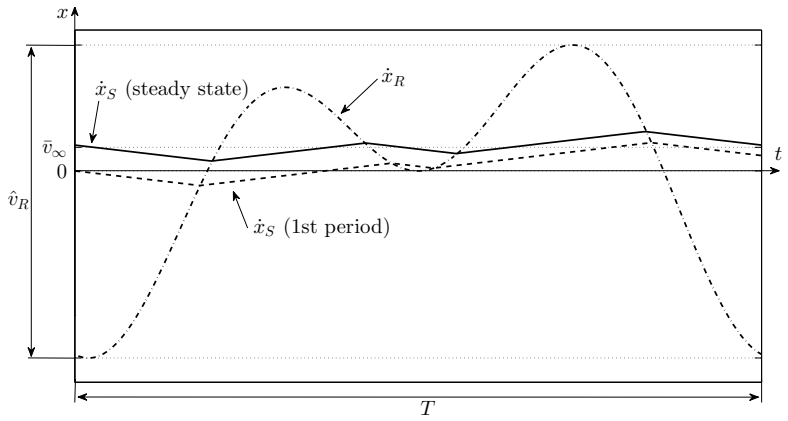

Figure 8: Velocities of rod and slider, excitated with a frequency-limited signal ($n = 2$, no σ factors), shown for the first period ($p = 1$) and for a period in steady state ($p \to \infty$).

The same argumentation shows that the course of the slider velocity at start-up is also qualitatively uninfluenced by a change of $\hat{x}_R$. This means that the number of periods p_q until the required degree of approximation to the steady state velocity is reached is constant. From (40) follows for the start-up time $T \cdot p_q$:

$$T \cdot p_q \propto \sqrt{\hat{x}_R} \tag{42}$$

To achieve high velocities it is therefore advisable to use actuators with large stroke. But – at least for non-resonant operation – the higher the stroke of an actuator is, the lower its maximum allowed operating frequency usually is. For example, the maximum allowed frequency for longitudinal actuators is often determined as a fixed percentage of the first resonance frequency. This is inversely proportional to the actuator length, which in turn is directly proportional to the actuator stroke. Thus

$$f_{\text{allowed}} \propto \frac{1}{\hat{x}_R}. \tag{43}$$

This maximum allowed frequency falls faster with rising actuator stroke than the maximum signal frequency, which falls with the inverse of the square root of the actuator stroke, cp. (37). Figure 9 visualises this relation. Right of the dotted line in the figure, the velocity of an inertia motor is impaired by the maximum frequency allowed for the actuator. Left of the dotted line the bandwidth of the actuator cannot be fully used. To reach the maximum velocity possible, making full use of the actuator capabilites, the motor should thus be designed so that $f_{\max} = f_{\text{allowed}}$.

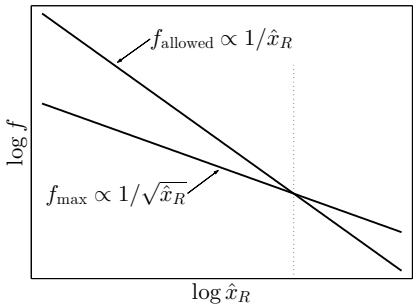

Figure 9: Schematic visualising the dependance of $f_{\max}$ and f_{allowed} on $\hat{x}_R$

The theoretical result that high stroke actuators allow higher motor velocities is supported by the fact that almost all inertia motors achieving high (here: $20\,\mathrm{mm\,s^{-1}}$ or larger) velocities use large actuator strokes achieved either by resonance effects [22, 3, 23, 26] or by mechanical amplification using compliance mechanisms [27] or bending actuators [28, 29, 30]. As far as known to the authors, only the motor by Okamoto and Yoshida [1] reaches such velocities with an un-amplified multilayer actuator.

9. Conclusions

Using the example of a translational inertia motor excited by an ideal displacement signal, it was found in the first part of this contribution [4] that there are four different modes of operation of inertia motors which are differentiated by two criteria: discrete or continuous modes of operation, and stick-slip or slip-slip operation. One major result of the investigation of the motor performance

was that the maximum velocity reachable in stick-slip operation and/or with discrete steps is limited principally, while continuous slip-slip operation allows very high velocities.

In this part, it was shown that continuous slip-slip operation is also the one that can best be achieved with real actuators. Even with signals containing harmonics of relatively low frequency only, velocities higher than the theoretical maximum for stick-slip operation can be achieved.

A comparison of different signals showed that the highest velocity and the smoothest slider motion are achieved with a signal containing only two harmonics, and a fundamental frequency as high as possible. Especially for signals with only two harmonics, using Lanczos' σ factors for calculating the amplitudes of the harmonics contained in the excitation signal drastically increases the steady state velocity, the durability, and the power requirement of the motor and also has a positive effect on the smoothness of the motor motion. The only disadvantage of using these factors is a small increase in start-up time.

For the investigated driving signals, the motor velocity is proportional to the square root of the actuator stroke. To build high velocity inertia motors it is therefore recommendable to use actuators with large stroke and to drive them with a signal consisting of two harmonics, ideally making use of resonance effects, at a high fundamental frequency. High resonance frequencies and large stroke are conflicting goals in the design of piezoelectric actuators. For non-resonant operation it was shown that inertia motors should ideally be operated so that the highest frequency component of the driving signal equals the maximum frequency allowed for the piezoelectric actuator.

As the knowledge about the advantages of slip-slip operation of inertia motors is growing and spreading, the authors expect that the number of dedicated slip-slip inertia motors will grow significantly in the near future, further widening the field of application of inertia motors.

Vitae

Matthias Hunstig studied mechanical engineering at the University of Paderborn and graduated with distinction at the end of 2007. Since then he is a research assistant at the chair for mechatronics and dynamics at the University of Paderborn. He started working on different piezoelectric systems as a student, developing energy harvesters and active vibration damping systems. His current main research interests are piezoelectric drives and energy harvesting.

Tobias Hemsel studied mechanical engineering at the University of Paderborn. After graduating in 1996 he was a research assitant at the Heinz Nixdorf Institute of the University of Paderborn and received his PhD in 2001. Since then he is engineering head at the chair for mechatronics and dynamics at the University of Paderborn. His research interests focus on sensors and actuators, especially piezoelectric systems.

Walter Sextro studied mechanical engineering at the University of Hanover and Imperial College in London. After graduating, he designed and optimized

drill strings for Baker Hughes Inteq research in Celle, Germany and Houston, Texas. He received his PhD from the University of Hanover in 1997. Subsequently, he qualified as a professor in the field of mechanics and published his habilitation thesis. In 2004 he was appointed as a professor at the institute of mechanics and gear trains at the Technical University of Graz, Austria. Since 2009 he leads the chair for mechatronics and dynamics at the University of Paderborn.

[1] Y. Okamoto, R. Yoshida, Development of linear actuators using piezoelectric elements, Electronics and Communications in Japan, Part 3 81 (1998) 11–17. Translated from Denshi Joho Tsushin Gakkai Ronbushi, Vol J80-A, No. 10, October 1997, pp. 1751–1756.

[2] J. Lee, W. S. Kwon, K. Kim, S. Kim, A novel smooth impact drive mechanism actuation method with dual-slider for a compact zoom lens system, Review of Scientific Instruments 82 (2011) 085105.

[3] T. Nishimura, H. Hosaka, T. Morita, Resonant-type smooth impact drive mechanism (SIDM) actuator using a bolt-clamped langevin transducer, Ultrasonics 52 (2012) 75–80.

[4] M. Hunstig, T. Hemsel, W. Sextro, Stick-slip and slip-slip operation of piezoelectric inertia drives – part I: Ideal excitation, Sens. Actuators, A (2012). Accepted 2012-11-06 (reference SNA_8081).

[5] M. Hunstig, T. Hemsel, W. Sextro, Improving the performance of piezoelectric inertia motors, in: ACTUATOR 2010 Conference Proceedings, Bremen, pp. 657–661.

[6] M. D. Greenberg, Advanced engineering mathematics, Prentice Hall, Englewood Cliffs, NJ, 1988.

[7] E. Hewitt, R. E. Hewitt, The Gibbs-Wilbraham phenomenon: An episode in fourier analysis, Archive for History of Exact Sciences 21 (1979) 129–160.

[8] R. W. Hamming, Numerical Methods for Scientists and Engineers, Dover, 2 edition, 1986.

[9] C. Edeler, S. Fatikow, Open loop force control of Piezo-Actuated Stick-Slip drives, International Journal of Intelligent Mechatronics and Robotics 1 (2011) 1–19.

[10] C. Cheng, S. Hung, The design and characteristic research of a dual-mode inertia motor, in: 2011 IEEE/ASME International Conference on Advanced Intelligent Mechatronics (AIM), IEEE, 2011, pp. 605–610.

[11] C. Belly, T. Porchez, M. Bagot, F. Claeyssen, Improvement of linear and rotative stepping piezo actuators using design and control, in: ACTUATOR 2012 Conference Proceedings, Bremen, Germany, pp. 246–249.

[12] M. Suzuki, H. Hosaka, T. Morita, Resonant-type smooth impact drive mechanism actuator with two langevin transducers, Advanced Robotics 26 (2012) 277–290.

[13] M. Pak, A. Nasseri, Load-velocity characteristics of a stick-slip piezo actuator, in: ACTUATOR 2012 Conference Proceedings, Bremen, Germany, pp. 755–756.

[14] K. Nakamura, M. Kurosawa, H. Kurebayashi, S. Ueha, An estimation of load characteristics of an ultrasonic motor by measuring transient responses, Ultrasonics, Ferroelectrics and Frequency Control, IEEE Transactions on 38 (1991) 481–485.

[15] T. Uchiki, T. Uchiki, T. Nakazawa, T. Nakazawa, K. Nakamura, M. Kurosawa, S. Ueha, Ultrasonic motor utilizing elastic fin rotor, in: Ultrasonics Symposium, 1991. Proceedings., IEEE 1991, pp. 929–932 vol.2.

[16] K. Asai, M. Kurosawa, T. Higuchi, Evaluation of the driving performance of a surface acoustic wave linear motor, in: 2000 IEEE Ultrasonics Symposium, volume 1, pp. 675 –679 vol.1.

[17] C. Edeler, Measurements and potential applications of Force-Control method for Stick-Slip-Driven nanohandling robots, Key Engineering Materials 467-469 (2011) 1556–1561.

[18] C. Edeler, Modellierung und Validierung der Krafterzeugung mit Stick-Slip-Antrieben für nanorobotische Anwendungen, Dissertation, Carl von Ossietzky Universität Oldenburg, 2011.

[19] P. Pertsch, S. Richter, D. Kopsch, N. Krämer, J. Pogodzik, E. Hennig, Reliability of piezoelectric multilayer actuators, in: ACTUATOR 2006 Conference Proceedings, Bremen, pp. 527–530.

[20] E. Rabinowicz, Friction and Wear of Materials, John Wiley & Sons, Inc., 2 edition, 1995.

[21] R. Bansevicius, V. Blechertas, Multi-degree-of-freedom ultrasonic motors for mass-consumer devices, Journal of Electroceramics 20 (2008) 221–224.

[22] B. Koc, Piezoelectric motor, operates by exciting multiple harmonics of a square plate, in: ACTUATOR 2010 Conference Proceedings, Bremen, pp. 194–197.

[23] T. Morita, H. Murakami, T. Yokose, H. Hosaka, A miniaturized resonant-type smooth impact drive mechanism actuator, Sensors and Actuators A: Physical 178 (2012) 188–192.

[24] B. Richter, J. Twiefel, J. Wallaschek, Piezoelectric equivalent circuit models, in: S. Priya, D. J. Inman (Eds.), Energy Harvesting Technologies, Springer US, Boston, MA, 2009.

[25] H. G. Natke, Einführung in Theorie und Praxis der Zeitreihen- und Modalanalyse: Identifikation schwingungsfähiger elastomechanischer Systeme, Vieweg, Braunschweig; Wiesbaden, 3 edition, 1992.

[26] S. Tuncdemir, Y. Bai, K. Uchino, Parametric optimization of rotary-linear dual function ultrasonic motor, in: ACTUATOR 2012 Conference Proceedings, Bremen, Germany, pp. 242–245.

[27] C. Belly, F. Claeyssen, R. Le Letty, T. Porchez, Benefits from amplification of piezo actuation in inertial stepping motors and application for high-performance linear micro motors, in: ACTUATOR 2010 Conference Proceedings, Bremen, pp. 198–201.

[28] H. Wörn, R. Munassypov, S. Fatikow, Actuation principle and motion control of a Three-Legged piezoelectric micromanipulation robot, in: ACTUATOR 98 Conference Proceedings, Bremen, pp. 203–206.

[29] L. Sun, Y. Zhang, P. Sun, Z. Gong, Study on robots with PZT actuator for small pipe, in: Proceedings of 2001 International Symposium on Micromechatronics and Human Science, pp. 149–154.

[30] D. Paik, K. Yoo, C. Kang, B. Cho, S. Nam, S. Yoon, Multilayer piezoelectric linear ultrasonic motor for camera module, Journal of Electroceramics 22 (2009) 346–351.